Nuclear Instruments and Methods in Physics Research A 624 (2010) 498–503

Contents lists available at ScienceDirect

Nuclear Instruments and Methods in Physics Research A

journal homepage: www.elsevier.com/locate/nima

Measurement results from an avalanche amplifying pnCCD for single photon imaging

I. Ordavo [a,d,*], R. Hartmann [a,d], P. Holl [a,d], A. Irlbeck [b,d], G. Lutz [a,d], R.H. Richter [c,d], G. Schaller [c,d], H. Soltau [a,d], L. Strüder [b,d]

[a] PNSensor GmbH, Römerstr. 28, D-80803 München, Germany
[b] Max-Planck-Institut für extraterrestrische Physik, Giessenbachstr. D-85748, Garching, Germany
[c] Max-Planck-Institut für Physik, Föhringer Ring 6, D-80805 München, Germany
[d] Max-Planck-Institut-Halbleiterlabor, Otto-Hahn-Ring 6, D-81739 München, Germany

ARTICLE INFO

Available online 25 May 2010

Keywords:
Single photons
Avalanche
pnCCD
Geiger mode
HTRA
High QE

ABSTRACT

The company PNSensor and the MPI Semiconductor Laboratory are developing and have produced first prototypes of pnCCDs with an avalanche readout which aim at single photon sensitivity in the visible wavelength range. This resolution is provided by an avalanche diode integrated in the readout chain of every CCD column. The diode features a new topology and can collect signal electrons from the CCDs' depleted buried channel. The pixel-structure has been derived from pnCCDs and was optimized for lowest leakage current and for compatibility with the avalanche structures. All advantages of the pnCCDs are maintained, including high quantum efficiency (between 80% and 100%), high frame rate (up to 1000 frames/s) and low leakage current. Possible applications are in the field of High Time Resolution Astrophysics (HTRA). There, fast imaging of faint objects in the visible, such as, e.g. close binary stars or fast rotating neutron stars, requires single photon sensitivity and high frame rates. We present results from proof-of-principle tests carried out on first laboratory prototypes of such devices.

1. Introduction

The MPI Semiconductor Laboratory together with PNSensor have developed CCDs with back illumination, full depletion and pn-junctions in every active element. They have outstanding characteristics: high-speed readout with up to 1100 frames/s, wide spectral sensitivity from the near infrared to X-ray energies of 25 keV with quantum efficiencies above 90% from 0.3 to 11 keV [1] and between 80% and 100% in the visible range, radiation hardness, and low noise. The applications include X-ray focal plane instrumentation (e.g. on the XMM-Newton and the future eROSITA satellites) and high speed optical imaging (e.g. for High Time Resolution Astrophysics [5]).

The concept of a novel CCD with an electron-multiplying readout is presented. Every CCD column features a passively quenched avalanche cell designed to collect signal electrons from the depleted detector volume (refer to Section IV of [2] for the technological details). The avalanche anode is directly coupled to the gate of an FET realized on-chip, which provides a low impedance coupling to the external amplification stage. The pixel-structure has been derived from pnCCDs and was optimized for lowest leakage current and for compatibility with the avalanche structures. All advantages of pnCCDs are maintained and include an anti-reflective-coating (ARC) applied to maximize quantum efficiency in an application specific wavelength range. A proof of principle production of the new avalanche diode has already been completed successfully, results are published in Refs. [2,3].

2. The avalanche pnCCD: general concept

The device concept is based on the combination of a back-illuminated pnCCD with an avalanche cell as the readout node for each column. Referring to Fig. 1, two main regions can be distinguished. The pixellated sensitive area consists of a three-phase CCD structure where all active elements are reverse-biased pn-junctions for low-noise operation. By proper biasing and switching of the registers, signal charge in each column is shifted toward the corresponding readout node. This is an avalanche cell designed to work in Geiger mode with a multiplication factor between 10^5 and 10^6. Quenching of the avalanche current results from the voltage drop across an integrated high-value poly-silicon resistor (typically $>1\,M\Omega$) which reduces the current below the

* Corresponding author at: PNSensor GmbH, Römerstr. 28, D-80803 München, Germany.
E-mail address: ior@hll.mpg.de (I. Ordavo).

0168-9002/$ - see front matter © 2010 Elsevier B.V. All rights reserved.
doi:10.1016/j.nima.2010.04.155

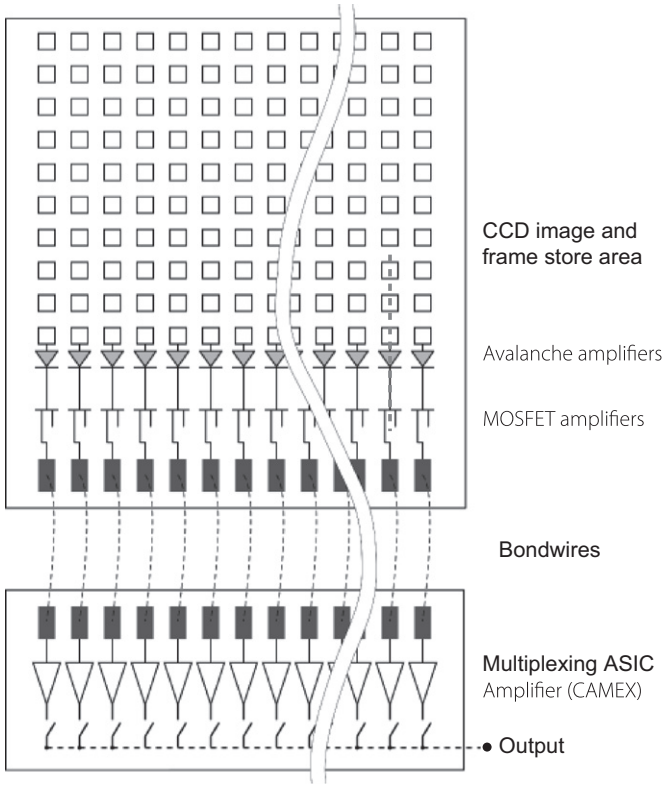

Fig. 1. Schematic picture of an avalanche amplifying pnCCD. Every column in the sensitive region (CCD image and frame store area) is coupled to an avalanche diode operated in Geiger mode. The signal is buffered by an on-chip source-follower wire bonded to an ASIC amplifier.

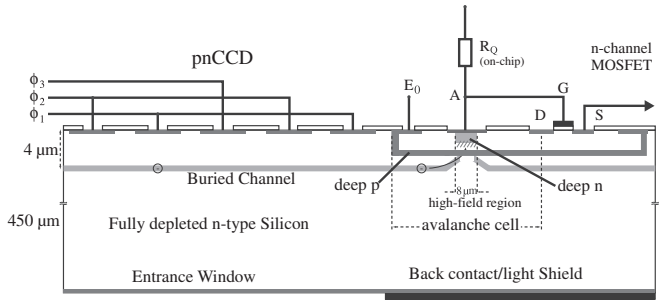

Fig. 2. Cross-section view along the dashed line in Fig. 1. The transfer direction for signal electrons is from left to right.

latching value of 20 µA. The voltage signal is buffered by an on-chip source-follower, also one per column. The output of the buffering stage is wire-bonded to the CAMEX [4] multiplexing ASIC for further signal amplification and shaping.

Fig. 2 shows a cross-section along an arbitrary column near the readout region. The radiation impinging onto the sensitive area through the homogeneous entrance window generates electron–hole pairs in the 450 µm thick, fully depleted silicon bulk. While holes drift toward the p^+ contact, electrons are collected in the potential minimum created by a 4 µm deep n-type buried channel. Shifting to the next register occurs by lowering the potential barrier for electrons in the transfer direction. Eventually, at the end of the CCD register array, electrons are attracted into the high field region by the about 15 V more positive potential of the deep p-type avalanche cathode. Even a single electron will be able to trigger an avalanche multiplication with high probability. Note that the readout region is insensitive to incoming optical radiation due to an aluminum layer shield on the back-side.

3. Proof of principle tests on X-ray pnCCD in avalanche technology

Although avalanche CCDs share many features with X-ray pnCCDs produced so far, they are substantially new devices. This is because in order to meet the new technological constraints dictated by the realization of the avalanche cell, some major changes in the device topology were adopted. This fact led to the necessity of testing the basic device functionality, a task which is not easily accomplished by using an avalanche-based readout. Dedicated test structures were therefore designed and processed on the same wafer along with avalanche devices. In particular, pnCCDs with standard non avalanche anode readout and an MOS-based clear structure were realized and tested. The device active region (image and frame-store area) are the same as for avalanche CCDs, while in the readout region, the high-field implants have been omitted (see Fig. 3 compared to Fig. 2) in favor of a shallow n^+ collecting anode and no quenching resistor is used. As can be seen from the top-view of Fig. 4, the anode is connected via a metallization layer to the gate of a n-type MOSFET embedded in a p-well and operated as source follower with external current load. Moreover, each channel features a sideward

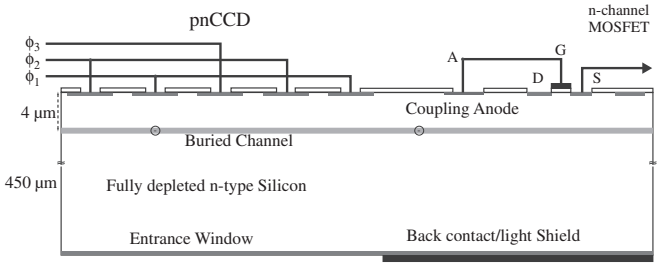

Fig. 3. Cross-section view of a simplified device. The high-field implants and the quenching resistor are omitted to test basic functionality and perform spectroscopic measurements.

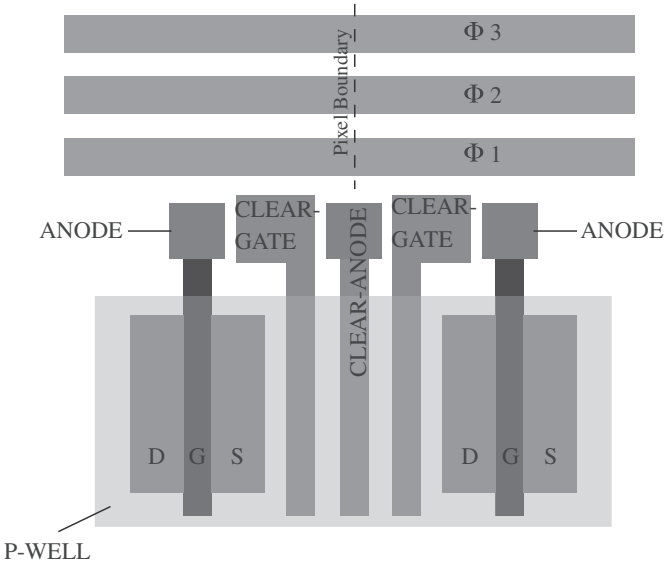

Fig. 4. Schematic top view showing the readout region of a simplified pnCCD produced in the new avalanche technology. Charge transfer direction is top down. The collecting anode is coupled to the transistor gate, one transistor per column. Two readout anodes share a common clear contact located in between.

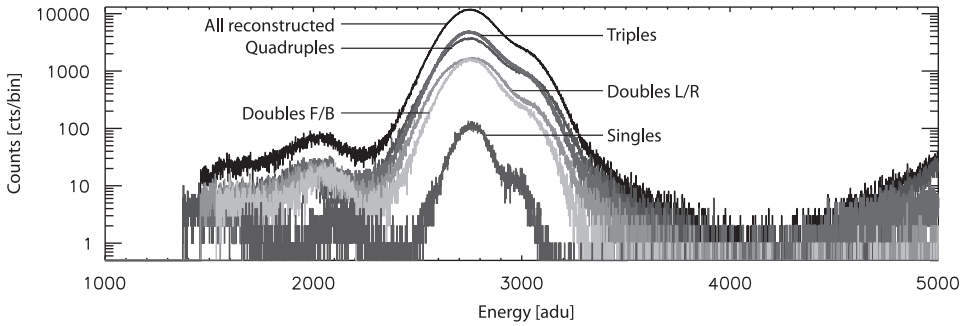

Fig. 5. Energy spectra of an ^{55}Fe photon source obtained with a 51 μm × 51 μm pixel size small area (176 rows × 132 columns) pnCCD produced with avalanche technology. The Mn-K_α and Mn-K_β peaks are merged for all split patterns due to the high transistor noise. The different histograms correspond to different patterns of split events, with the following meaning from higher to lower peak height: all recombined events, triples, quadruples, doubles forward/backward and left/right and singles. The most resolved spectrum is that of single events, where *S/N* reaches its maximum.

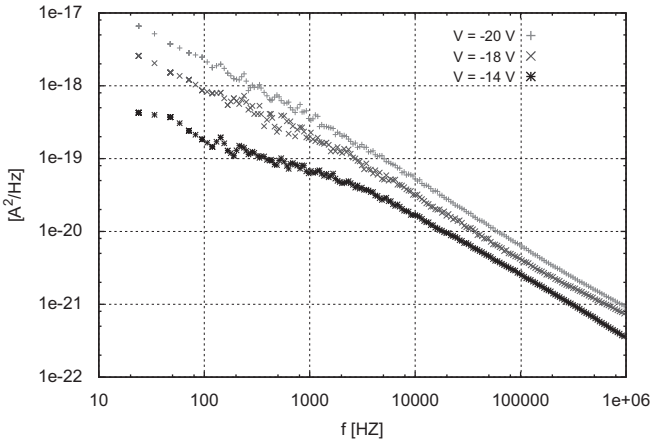

Fig. 6. Power spectral densities of the front-end transistor used as first amplifier. The curves correspond to three different voltages of the embedding p-type well.

MOS gate, while a common reset anode is shared between two adjacent channels. A periodic pulse applied to the clear-gate ensures the removal of the charge accumulated on the MOSFET gate, usually after each frame is readout.

The overall functionality and spectroscopic performance of the device were tested under flat-field illumination with X-ray photons produced by an ^{55}Fe source. pnCCDs with 51 μm × 51 μm pixel size and 176 rows × 132 columns were used for such testing purposes. The resulting spectra in logarithmic scale from a typical measurement are shown in Fig. 5. The Mn-K_β, located at 6.5 keV is distinguishable as a shoulder right of the K_α peak centered at 5.9 keV. The different histograms correspond to different patterns of split events which are dominant for this pixel size. The small percentage of single events (lowest curve) yields the best *S/N* ratio which results in a more distinct separation between the two peaks. An estimation of the noise contribution from the energy resolution led to an ENC between 30 and 100e^- RMS with a strong dependance of this figure on the transistor p-well voltage. This fact was confirmed by measurements of the noise spectral power density carried out on isolated test transistor structures. The plot in Fig. 6 shows such a measurement for three different p-well voltages. The trend toward better noise performance with increasing p-well voltage is clearly seen. This fact can be qualitatively understood by assuming that a trapping of charge carriers in the transistor channel is responsible for $1/f$ noise. From the transistor transfer curves (Fig. 7) can be seen that a rising well potential, for constant load current, causes the gate-source voltage to drop, thus pushing the conductive electrons away from the surface, where trap density is highest. However, at well voltages more positive than −10 V, punch-through effects with surrounding p-implants arise, preventing from a further lowering of the noise. It is worth pointing out the fact that avalanche CCDs are not intended to perform as spectroscopic devices, since their response to signal electrons is highly non-linear. An avalanche cell, when operated in Geiger mode, is a binary device generating 10^5 to 10^6 electrons, independent of the number of incoming electrons, thus reaching very high *S/N* ratios, even with 100e^- ENC.

The other fundamental parameter which can be extracted from these first measurements is the capability of the CCD to shift the charge from pixel to pixel without losses, expressed by its Charge Transfer Efficiency (CTE, i.e. the fraction of electrons successfully transferred from one pixel to another). The best CTE value from flat-field measurements with ^{55}Fe X-ray photons at −60 °C has been found to be 99.995%. This is compatible with a shallower buried channel technology where the electrical isolation of signal charge from the surface is more critical. This figure has to be compared to conventionally processed pnCCDs, where the charge transfer takes place about 3 μm deeper and a CTE of 99.9996% is typical [2].

As a conclusion, tests carried out on standard X-ray pnCCDs produced with avalanche technology have shown the device capability to store, shift and amplify the charge generated by impinging radiation, enabling further testing of full featured avalanche devices.

4. Avalanche amplifying pnCCDs under test

Before testing the device in its full functionality, some preliminary investigations had to be made.

4.1. Pulse waveform characteristics and sampling strategy

The output of every pnCCD column is directly coupled to the input of a CMOS Amplifier and Multiplexer (CAMEX [4]) application specific integrated circuit (ASIC) via an on-chip nMOSFET biased with an external current load (see Fig. 8). This kind of amplifier was designed to deliver the voltage difference between two successive 8-fold correlated double sampling (CDS) steps: the first performed just before the charge is shifted to the readout anode, and the second shortly thereafter. This readout scheme is best suited for conventional pnCCDs, where the charge collected on the transistor gate stays there until it is actively removed by a clear structure (see beginning of Section 3); the voltage at the CAMEX input is in this case a step-like function. On the other side, some care has to be taken when dealing with waveforms originating from passively quenched avalanche

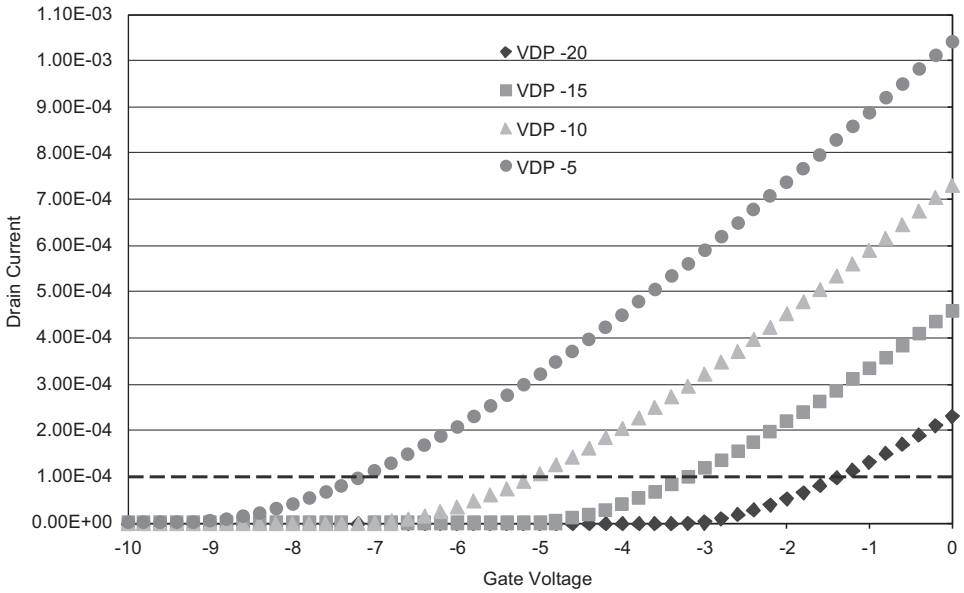

Fig. 7. Input characteristics of the front-end transistor used as the first amplification stage in source-follower configuration with constant current load. The strong steering power of the deep p-doped well is accounted for by the modulation in threshold voltage of over 10 V. The constant bias current level of 100 μA is indicated by the dashed line.

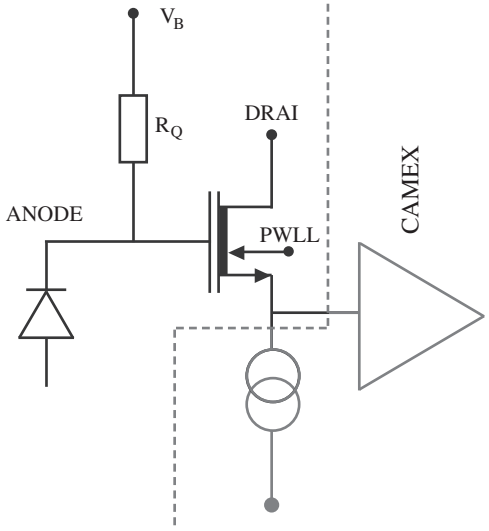

Fig. 8. Schematic diagram showing the readout chain of an arbitrary CCD column. The front end transistor is working as source follower and coupled to the CAMEX amplifier.

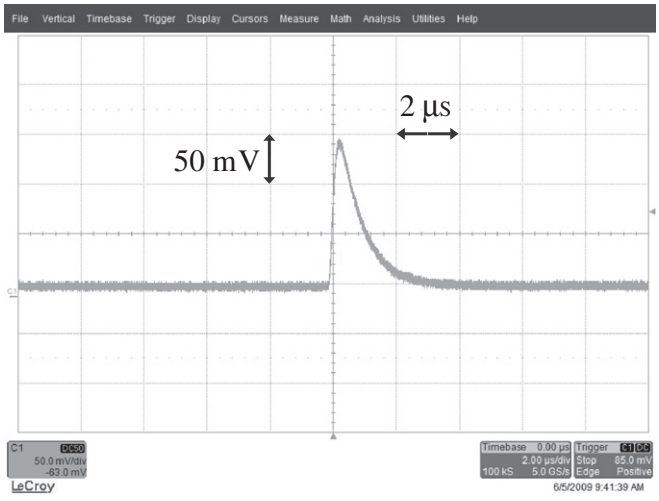

Fig. 9. Pulse waveform of an avalanche generated by a dark electron.

diodes, where the steady state voltage of the cell is restored within few microseconds. Such an amplifier is clearly not suited for very fast signals and is used in this context only for preliminary test purposes. The voltage pulse of a firing avalanche cell can be obtained at the input of the CAMEX by switching CDS off and disabling the channel multiplexing feature, hence looking at the output of one channel at a time (for the sake of convenience we call this readout setup continuous locked mode or CLM). By rising the voltage above breakdown, avalanche signals generated by dark electrons in the high field region are expected. A typical dark pulse obtained in the CLM is shown in Fig. 9. The cells were all biased in parallel at 4 V over their breakdown voltage at −60 °C and the avalanche was quenched by a 2 MΩ resistor. To be noted is the fast quenching mechanism that restores the steady voltage within 2 μs.

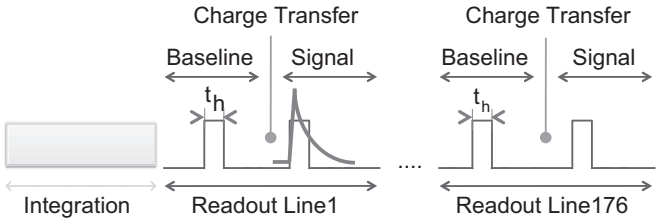

Fig. 10. Time structure of a whole frame cycle. After the charge collection time, the 132 pixels of the first CCD row are processed in parallel. A single sample placed immediately after the charge shift is enough to capture most of the fast decaying avalanche pulse, while another one is needed to set the baseline of the system.

In contrast to dark pulses, the arrival time of signal electrons at the anode is known ahead of time and a single sample can be placed after the charge is shifted onto the anode, where a significant part of the pulse is still present (see Fig. 10). Because of

the fast decay, any other subsequent sample would not add significant information and would rather increase the dark-count probability (see Section 4.2). Another sample is needed to set the baseline of the output before the charge shifting. In the case that signal electrons are transferred from the CCD into the high field region, the instant (T_{tr}) when the charge is transferred from the last register to the anode and the time where the corresponding avalanche pulse occurs (T_s) should be time correlated. To perform such a measurement, the CLM was used and a trigger signal with a fixed offset with respect to T_{tr} was chosen as a reference on one channel of a digital oscilloscope (see Fig. 11). On the other channel, where the avalanche has to be detected, a threshold is applied and whenever an avalanche occurs, their time difference (delay) is stored in a histogram. The result is presented in Fig. 12. The plot shows the absolute number of counts against the time difference $(T_{tr}-T_s)+T_{off}$, where T_{off} is a constant offset, while the CCD was illuminated uniformly with light. Note that the distribution is asymmetric: this is due to the fact that the avalanche signals are correlated with the charge transfer and cannot occur ahead of this occurrence but only thereafter. The presence of a peak indicates that electrons generated in the CCD bulk by impinging radiation effectively reach the high field region and give rise to avalanche multiplication.

4.2. Dark rate of single cells and bulk contribution

Investigation of the dark rate of single avalanche cells was performed on test structures with 9 μm high-field region diameter reproducing a two-channel avalanche CCD readout, with the CCD active area and register structure omitted (see Fig. 13). The potential distribution is such that electrons generated within the area outside the cells flow to a positively biased bulk contact and do not contribute to dark signals. This way, only electrons thermally generated within the high field region of the cell contribute to the dark current. The dark rate decays exponentially with temperature as expected from the Shockley–Hall–Read (SHR) generation model which predicts a dark rate dependence of the form $J_g \propto T^{3/2}\exp(-E_g/2kT)$. The discrepancy of measured values from the predictions at lower temperature can be explained by diffusion of electrons into the high field region, tunneling or after-pulsing. However, within the temperature operating range of the CCD, between −60 and −80 °C, and at typical operating conditions, the expected dark rate of a single avalanche cell will slightly exceed 100 counts per second. Moreover, at −80 °C and moderate biasing, the dark rate per cell can be extrapolated to less than 10 counts per second (Fig. 14). This value is further suppressed by the sampling procedure of the CAMEX. Since the amplifying chain is active only during the sampling phase (baseline+signal), we have to find out the effective total time in which the output is enabled (or high). Referring to a full frame readout, after the charge collecting time (see Fig. 10), the 132 pixel of the first CCD line are processed in parallel. Since the avalanche cells can fire independently, the probability to have a dark count from any of them, during the first run, is multiplied by the number of CCD columns. The processing is repeated for all CCD rows, such that the total dark counts per frame are given by the formula $DR \cdot (n_r \cdot n_c \cdot 2t_h)$, where DR is the dark count rate of a single cell, n_r and n_c the number of CCD rows and columns, respectively, t_h the sample high time (typically 500 ns) and two samples per line processing are assumed. The overall contribution of the avalanche cells to the dark current is estimated to be as low as 2 dark event per frame at −60 °C and 8 V overbias for a 176 × 132 pixel CCD.

This number has to be compared with the measured bulk contribution from Ref. [6] at the same temperature. At the readout speed of 100 Hz, a bulk-generated ENC of 36e⁻ RMS per frame is

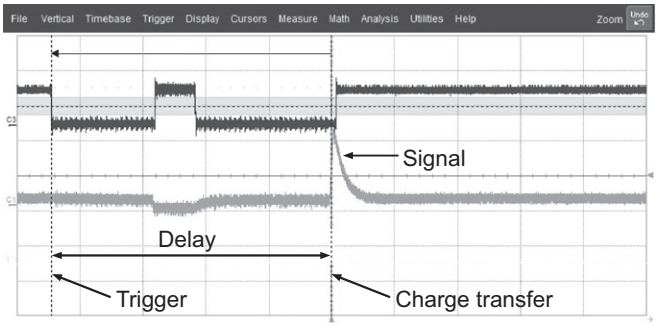

Fig. 11. Snapshot from a digital oscilloscope illustrating the principle of the time-correlated measurement. Refer to text for the details.

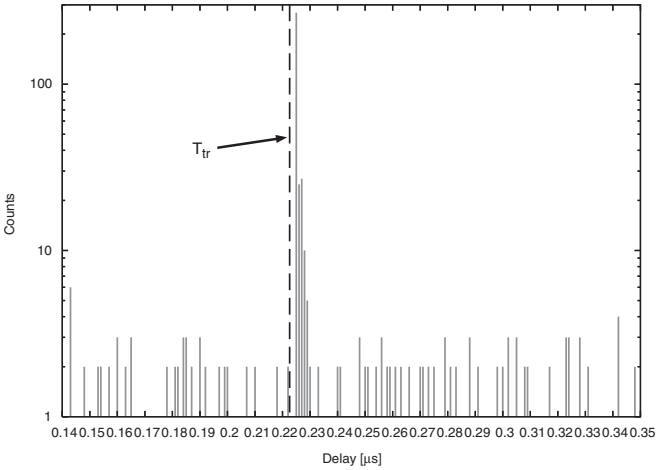

Fig. 12. Measurement of the time correlation between charge shifting and avalanche signal. Asymmetry in the time distribution is due to the fact that the avalanche signals are correlated with the charge transfer (T_{tr}) and cannot occur ahead of this.

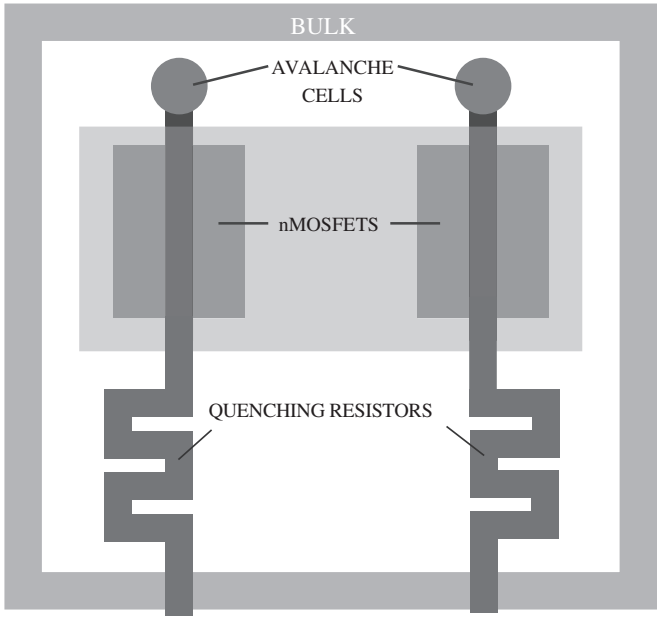

Fig. 13. Schematic top view of a test structure with cells of 9 μm diameter for investigating the dark current contribution of single readout cells. The bulk contact is the most positive one such that electrons from the surrounding area outside the cells do not contribute to dark counts.

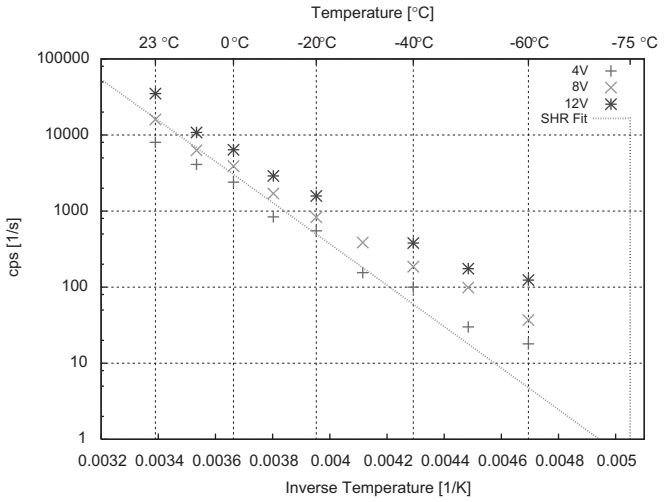

Fig. 14. Dark rate dependance on temperature and overbias for a single avalanche cell with 9 μm diameter. Exponential decay down to 30 counts/s has been measured. The data points follow SHR generation (linear fit at 8 V overbias) only for the higher temperature regime with a progressive departure of the experimental data from the model at lower temperatures.

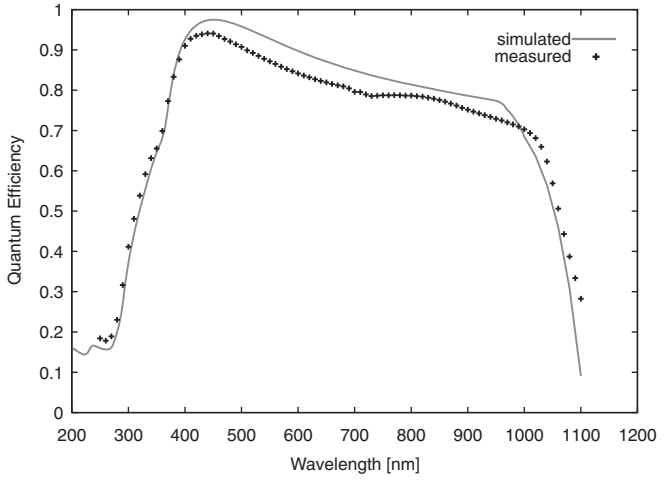

Fig. 15. Simulated (solid curve) and measured (points) quantum efficiency of avalanche pnCCD entrance window with anti-reflective-coating.

expected, showing that at this moderate speed the cell dark rate can be neglected. For faster readout (e.g. at 1 kHz), the two contributions become comparable and the cell rate must be taken into account.

4.3. Quantum efficiency

Thanks to the established double sided silicon wafer technology developed at the Semiconductor Laboratory, full control of the back-side processing is achieved. Since our detectors are back illuminated, this translates into outstanding properties not only in terms of homogeneity of the entrance window but also in terms of optical sensitivity. As a consequence, a fill factor of 100% is a naturally given characteristic. Another benefit is the ability to control the thickness of dielectric layers in order to form Anti-Reflecting-Coatings (ARC) for different wavelengths. For the avalanche CCD production we opted for a broad band ARC, with peak efficiency around 450 nm. Values for this production were obtained by measuring the photo-current generated by a calibrated photodiode at different wavelengths and are shown in Fig. 15 (data points). The results are in good agreement with the performed simulations (solid line) in the wavelength range of interest from 400 to 1000 nm.

5. Summary and outlook

In this paper we have shown the results from preliminary tests of a new device that aims at imaging single photons in the optical range. The device concept and design is based on the established pnCCD technology developed at the Semiconductor Laboratory of the Max-Planck-Institut. Thanks to a double-sided processing and fully depleted silicon bulk, the outstanding properties of pnCCDs in terms of high quantum efficiency and low leakage current are maintained. Moreover, the single photon sensitivity is targeted by the integration of an avalanche cell in the readout chain of every column. First successful proof of principle tests have shown the overall capability of the CCD to collect, shift and amplify the charge. In particular, the basic mechanism of transferring the charge from the CCD bulk to the avalanche high field region has been proven successful by a time correlated measurement. Parameter optimization is ongoing and operation in low light conditions will be tested soon.

Acknowledgements

We would like to acknowledge Prof. M. Sampietro and Dr. G. Ferrari of the Politecnico di Milano and Dr. M. Porro for the competent support provided during the measurements of transistor noise spectra.

The project was supported by the Johannes-Heidenhain-Stiftung.

References

[1] N. Meidinger, et al., Proceedings of SPIE 6686 (XIII) (2007) 0H1.
[2] P. Holl et al., A new high-speed, single photon imaging CCD for the optical, in: Conference record of IEEE Nuclear Science Symposium, 2006.
[3] C. Merck et al., Back illuminated drift silicon photomultiplier as novel detector for single photon counting, in: Conference record of IEEE Nuclear Science Symposium, vol. 3, 2006, pp. 1562–1565.
[4] W. Buttler, et al., Nucl. Instr. and Meth. A 288 (1997) 140.
[5] S. Ihle et al., Optical test results of fast pnCCDs, in: Conference record of IEEE Nuclear Science Symposium, 2008.
[6] P. Holl, et al., pnCCDs for ultra-fast and ultra-sensitive optical and NIR imaging, in: Proceedings of the HTRA Workshop, September 2007, Edinburgh, AIP Conference Proceedings 984, 2008, pp. 115–120.